RAA 2020 Vol. **20** No. **3**, 35(14pp) doi: 10.1088/1674–4527/20/3/35

http://www.raa-journal.org *http://iopscience.iop.org/raa*

Research in Astronomy and Astrophysics

Searching for exoplanets by HEPS II. detecting earth-like planets in habitable zone around planet hosts within 30 pc

Zhou-Yi Yu, Hui-Gen Liu, Ji-Lin Zhou, En-Si Liang, Ming Yang, Hui Zhang and Jia-Cheng Liu

School of Astronomy and Space Science, Key Laboratory of Modern Astronomy and Astrophysics in Ministry of Education, Nanjing University, Nanjing 210093, China; *huigen@nju.edu.cn; zhoujl@nju.edu.cn*

Received 2019 May 22; accepted 2019 October 8

Abstract HEPS (Habitable ExoPlanet Survey) is a planning astrometry satellite that aims to find Earth-like planets in the solar neighbourhood. In this paper, we selected 140 planet harboring stars within 30 pc of the solar system to be potential targets for HEPS. We calculate the detection probability of the planet in habitable zone (HZ) for each system using the simulated data of astrometry measurements. For those host stars without planets in HZ, we inject an additional planet of 10 $M_\oplus$ in their HZs and check the stability of the systems. Considering five observation modes of different sampling cadence and total observation time, we obtain a table containing the total detection probability of the planets in HZs for all of the 140 selected systems. This paper provides a potential ranked list of target stars for HEPS, or other astrometric mission to detect Earth-like planets in the future. We also calculate an empirical fitted expression of the detection probability as a function of both sampling cadence and total observation time. We conclude a quantitative method to estimate the detection probability for certain planet hosts and observation modes via the empirical expression. We show the minimum requirements of both sampling cadence and observation time for Proxima Centauri, HD 189733 and HD 102365, if the detection probability of habitable-zone planets of these three systems needs to be 90%.

Key words: astrometry — stars: planetary systems — planets and satellites: detection — methods: numerical

1 INTRODUCTION

The launch of the Gaia satellite (Gaia Collaboration et al. 2016) marks a new era for detecting exoplanets using high-precision astrometry. Unlike traditional detecting methods, such as radial velocity (RV) and photometry, planet mass and orbital elements are simultaneously obtainable using astrometry measurements (Wright & Howard 2009). Gaia monitors the motions of billions of stars on the celestial plane with an unprecedented precision. For stars brighter than a G-band magnitude 12, a precision of 10.6 μas is achieved. Perryman et al. (2014) estimated that a total of 21 000 high-mass ($1 - 16\,M_{\rm Jupiter}$) exoplanets would be found after its 5-year mission time. However, detecting Earth-like planets is still challenging for Gaia; for example, an Earth-like planet in the habitable zone around a sun-like star at 10 pc requires a precision of 0.3 μas.

Finding nearby Earth-like planets is crucial to understanding the uniqueness of our solar system. Several Earth-like planets have already been detected by RV (Proxima b Anglada-Escudé et al. 2016; Barnard b Ribas et al. 2018) or photometry (Trappist-1 b,c Gillon et al. 2016), although these planets lack definitive mass information. Given the occurrence rate of Earth-like planets around GK dwarfs based on the Kepler mission (Burke et al. 2015) and the SAG-13 parametric model of planet occurrence rates, dozens of planets of this type within 30 pc should be present. Considering the detection probability and the required precision of RV or photometry, nearby Earth-like planets detected by astrometry are able to provide us with information of planetary mass and orbital elements, which is very important to study the habitability of these planets.

For the purpose of detecting Earth-like planets, space-based astrometry satellites with extremely high precision have already been proposed, such as NEAT (Malbet et al. 2012), SIM (Unwin et al. 2008), Theia (The Theia Collaboration et al. 2017), TOLIMAN (Tuthill et al. 2018) and MASS (Shao 2019), whose precisions were designed to reach sub-microarcsecond level. Simulations made by Unwin et al. (2008) demonstrated that 61% of all terrestrial planets within 30 pc could be detected by SIM, showing that detecting Earth-like planets in the solar neighborhood using astrometry is feasible.

The main scientific goal of a newly proposed space-based astrometry telescope, HEPS (Habitable ExoPlanets Survey), whose former name is STEP (Searching for Terrestrial Exo-Planet Satellite) (Chen et al. 2013), is to find habitable Earth-like planets in the solar neighborhood. This spacecraft is designed to operate for a 5-year mission time on a halo orbit at the L2 point of the Sun and Earth. With a 1.5-meter telescope steadily pointing to individual targets of careful selection, HEPS is able to achieve an astrometry precision as high as 0.3μas for stars brighter than V magnitude of 8. Unlike the observation mode of Gaia, HEPS only monitors specific targets. Its preliminary observation plan is to observe 200 targets with a cadence of 0.1 year during its mission time. An efficient target list is therefore very important for HEPS to yield fruitful results.

Previous works on selecting targets for astrometry missions mainly focus on calculating the signal-to-noise ratio (SNR) of the astrometry signals induced by Earth-like planets in each system (Malbet et al. 2012).

In this work, we adopt a more comprehensive method, where we fit the orbital elements of the planets in the HZ of each system using simulated astrometry data, and select our targets based on the fitting quality of the Earth-like planets.

The Kepler Space telescope finds that multi-planet systems are common based on existing data, and stars known to harbor planets have a high chance to have undetected planets. Therefore, we focus on systems listed in the NASA exoplanet archive and obtain their distance and proper motions from Gaia DR2 (Gaia Collaboration et al. 2018), which is a step forward from the first paper of this series, where only artificial data is used (Yu et al. 2019).

We aim to make a list of target stars within 30 pc for the HEPS mission, and rank these targets based on their detection probability ($P_{\rm HE}$).

This paper is arranged as follows. In Section 2 we discuss the standards of the chosen planetary systems and how we simulate and fit the planetary parameters. Section 3 presents our fitting results and the target list, and discusses the requirements of the HEPS mission. We discuss our results and conclude in Section 4.

2 SAMPLE SELECTION AND ASTROMETRY SIMULATION

2.1 Sample Selection

As mentioned in Section 1, Earth-like planets are more likely to be found in systems that are already known to harbor planets. Given the operation mode of HEPS, focusing on systems with known planets has a higher chance of yielding better results, which makes selecting targets from the NASA Exoplanet Archive[1] a reasonable choice.

We first rule out active stars in the exoplanet archive because stellar activities significantly increase observational noise, which hampers high precision astrometric measurements. Therefore, stars not satisfying $\log_{10} R_{\rm HK} < -4.35$ are excluded. Then, we exclude the binary systems with P-type planets because astrometry signals of the companion stars are very large and they make it difficult to correctly reveal the planet's signals.

In the first paper of this series, one of the most important factors influencing the detection probabilities of the planets is the SNR of the planetary astrometric signals (Yu et al. 2019), in which case a planet is detectable when the SNR of its maximum astrometric signal is larger than 3. To calculate the SNR of a planet, the first step is to calculate the maximum astrometric signal of the planet, A, which is in the form of

$$A \approx 3 \left(\frac{M_{\rm p}}{1M_{\oplus}}\right) \left(\frac{a_{\rm p}}{1{\rm AU}}\right) \left(\frac{M_{\rm s}}{1M_{\odot}}\right)^{-1} \left(\frac{d}{1{\rm pc}}\right)^{-1} \mu{\rm as}, \tag{1}$$

where M_s is the mass of the star, $M_\odot$ is the mass of the Sun, M_p is the mass of the planet, $M_\oplus$ is the mass of the Earth, a_p is the semi-major axis of the planet, and d is the distance of the target. The blue curve in the left panel of Figure 1 shows the calculated signal of a planet with a mass of $10\,M_\oplus$, orbiting a star of $1\,M_\odot$ at 1 AU, with different distances from the solar system. Based on Equation (1), when the distance is 30 pc, the maximum astrometric signal caused by the $10\,M_\oplus$ planet is $1\,\mu$as, which is just above the detection threshold considering the best precision of HEPS (0.3 μas). Therefore, we only select inactive planet hosts within 30 pc from the solar system in the exoplanet archive, based on the distance data of Gaia DR2. Selected systems will also benefit from high-precision astrometric measurements in terms of refining the parameters of known planets, which will lead to a better characterization of these systems.

In total, 144 planetary systems meet the above criteria, four of which are discarded since they lack information of either mass or effective temperature. Finally, 140 systems with measured planet masses are selected for further study. All of the information of selected stars, including their masses, proper motions and distances, is listed in Table 1. Note that after checking the binarity of stars in our sample, we find the minimum period of these binaries is over 70 years, which is much longer than the mission. The astrometry signal due to very long period stellar companions can be fitted linearly, which is degenerate with the

[1] `https://exoplanetarchive.ipac.caltech.edu/`

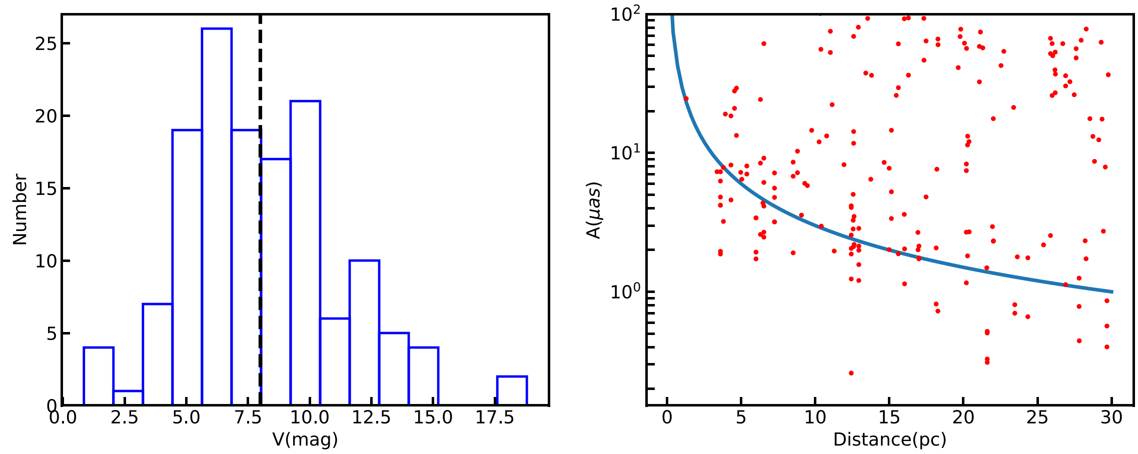

Fig. 1 The left panel of the figure is the distribution of the V magnitude of the 140 selected host stars of detected planets (see Sect. 2). The *black dashed line* represents $V = 8.0$, where the assumed astrometric precision is 1 μas. Nearly 53.9% of the stars are brighter than $V = 8.0$. The *red dots* in the right panel represent astrometric signals of all the detected planets around the planet hosts, according to Eq. (1). The *blue line* represents the astrometric signal of a 10 Earth-mass planet at 1 AU around a solar-mass star from 1 pc to 30 pc away.

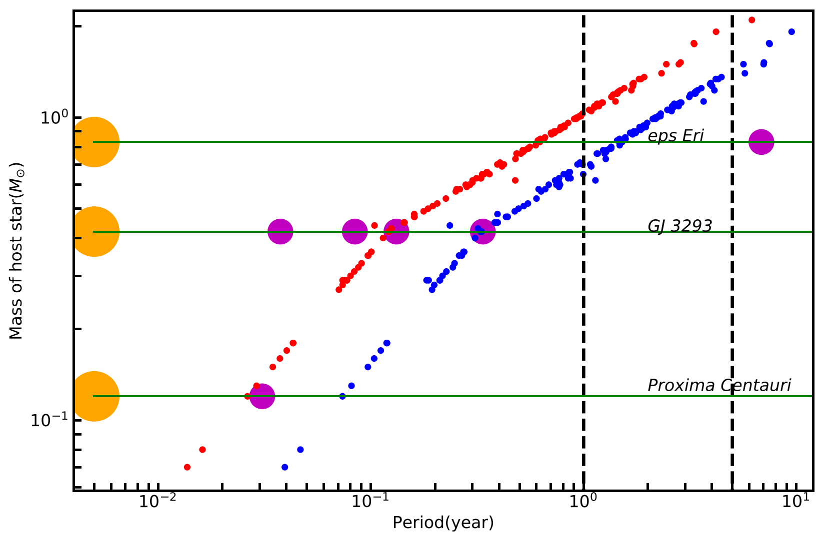

Fig. 2 The x axis represents the planets' period and the y axis is the mass of the host star. The *red* and *blue dots* show the inner and outer boundary of HZ, respectively. We also plot three typical planetary systems: Proxima Centauri, GJ 3293 and eps Eri. The *orange circle* is the mass of the host star. The *purple circles* represent the position of the planets already found in the system. We can see that the Proxima Centauri has one planet in the habitable zone. GJ 3293 has two planets in the habitable zone and two planets within the inner boundary, while eps Eri has one planet beyond the habitable zone.

stellar proper motion, while the signal due to stellar companions with shorter period can be corrected based on the precision of binary orbital parameters. In our simulation, we assume that all of the astrometry signals that are due to the companions are ignored, but we marked all these planet hosts with * in Table 1.

Based on the initial design of HEPS, the precision of the astrometric measurements is related to the V-band magnitude of the host stars, which can be expressed as

$$\sigma = \max[10^{\frac{V-8}{5}}, 0.3]\ \mu\mathrm{as}, \tag{2}$$

where σ is the standard deviation which is the larger value of the bracketed, and V is the V-band magnitude of the targets. The best precision is only reached when the stars are brighter than a magnitude of 5.39 in V-band. Note that this equation represents the noise of one measurements of the target after multi-exposure. The right panel of Figure 1 shows the histogram for all selected host stars based on their V-band magnitudes. For about 53% of the stars, HEPS is able to achieve a precision better than1 μas, since they are brighter than $V = 8$, whereas almost 17% of the stars are brighter than $V = 5.39$, for whom HEPS is

Table 1 Parameters of the Host Stars and the Detection Possibilities of the Earth-like Habitable Planets

Star Name	Mass ($M_\odot$)	$T_{\rm eff}$ (K)	μ_α (mas yr^{-1})	μ_δ (mas yr^{-1})	d (pc)	V (mag)	σ (µas)	ihz (AU)	ohz (AU)	N_{num}	$N_{\rm habi}$	$P_{\rm habi}$	$P_{\rm HP4}$: $P_{\rm D3}$	$P_{\rm D5/F10}$	$P_{\rm F20}$	$P_{\rm F50}$	$P_{\rm D8}$
HN Peg	1.1	5974.0	231.1	–113.1	18.13	5.95	0.389	1.137	1.995	1	0	1.0	**0.88**	**1.0**	**1.0**	**1.0**	**0.98**
HD 192310	0.8	5166.0	1242.5	–181.0	8.8	5.73	0.352	0.63	1.132	2	0	0.4115	**1.0**	**1.0**	**1.0**	**1.0**	**0.98**
HR 810	1.34	6167.0	333.8	219.5	17.33	5.41	0.303	1.667	2.913	1	0	0.299	0.14	**0.98**	**1.0**	**1.0**	**1.0**
HD 219134	0.81	4699.0	2074.5	294.9	6.53	5.57	0.327	0.66	1.209	6	0	1.0	**0.809**	**0.98**	**1.0**	**0.991**	**0.98**
tau Cet	0.78	5344.0	–1729.7	855.5	3.6	3.5	0.3	0.593	1.06	4	0	0.5725	**0.787**	**0.96**	**1.0**	**0.983**	**0.959**
61 Vir	0.94	5577.0	–1070.8	–1063.0	8.51	4.74	0.3	0.85	1.507	3	0	0.969	**0.553**	**0.96**	**0.966**	**0.991**	**1.0**
HD 19994*	1.36	6188.0	193.2	–69.3	22.54	5.06	0.3	1.715	2.996	1	0	0.0965	0.0	0.96	0.967	1.0	1.0
eps Eri	0.83	5084.0	–975.4	20.3	3.2	3.82	0.3	0.681	1.228	1	0	0.6605	**0.82**	**0.94**	**0.933**	**1.0**	**0.98**
HD 3651	0.88	5221.0	–462.1	–369.8	11.14	5.86	0.373	0.76	1.364	1	0	0.9625	**0.8**	**0.9**	**0.9**	**0.95**	**0.92**
GJ 86*	0.93	5182.0	2124.9	638.1	10.79	6.12	0.421	0.85	1.528	1	0	0.878	**0.8**	**0.9**	**0.867**	**0.9**	**0.92**
51 Peg	1.12	5793.0	207.4	62.1	15.47	5.5	0.316	1.191	2.1	1	0	0.9965	**0.76**	**0.9**	**0.833**	**0.967**	**0.94**
HD 26965	0.78	5072.0	–2240.5	–3421.4	5.04	4.43	0.3	0.601	1.085	1	0	0.994	**0.76**	**0.84**	**0.967**	**0.975**	**0.94**
tau Boo*	1.34	6400.0	–467.9	64.7	15.66	4.5	0.3	1.644	2.86	1	0	1.0	**0.32**	**0.84**	**0.667**	**0.8**	**0.72**
HD 177565	1.0	5778.0	–187.6	–367.0	16.93	6.16	0.429	0.951	1.676	1	0	0.995	**0.52**	**0.8**	**0.867**	**0.8**	**0.7**
GJ 504	1.22	6234.0	–336.7	190.6	17.54	5.22	0.3	1.376	2.402	1	0	0.9915	0.1	**0.8**	**0.833**	**0.917**	**0.92**
HD 102365	0.85	5630.0	–1530.6	402.9	9.29	4.91	0.3	0.693	1.227	1	0	0.9525	**0.88**	**0.78**	**1.0**	**0.975**	**0.9**
psi 1 Dra B	1.19	6212.0	33.8	–275.9	22.73	5.699	0.347	1.311	2.289	1	0	0.4465	0.1	**0.76**	**0.967**	**0.957**	**0.898**
HD 217107	1.0	5622.0	–7.1	–14.8	20.07	6.16	0.429	0.959	1.699	2	0	0.703	0.146	**0.68**	**0.9**	**0.915**	**0.898**
HD 1461	1.02	5765.0	417.9	–143.8	23.47	6.47	0.494	0.99	1.746	2	0	0.994	**0.277**	**0.66**	**0.862**	**0.914**	**0.816**
HD 69830	0.86	5385.0	278.8	–988.3	12.56	6.0	0.398	0.719	1.283	3	0	0.611	0.191	**0.66**	**0.828**	**0.948**	**0.735**
HD 190360*	0.99	5552.0	683.3	–525.7	16.01	5.73	0.352	0.944	1.676	2	0	0.659	0.104	**0.64**	**0.833**	**0.974**	**0.878**
rho CrB	0.89	5627.0	–198.5	–772.4	17.48	5.41	0.303	0.76	1.345	2	0	0.9145	**0.354**	**0.62**	**0.967**	**0.949**	**0.653**
HD 179949	1.21	6168.0	118.6	–102.2	27.48	6.25	0.447	1.359	2.375	1	0	0.998	**0.24**	**0.6**	**0.8**	**0.846**	**0.633**
HD 16417	1.2	5936.0	–18.5	–258.9	25.41	5.78	0.36	1.356	2.381	1	0	0.996	0.1	**0.6**	**0.667**	**0.889**	**0.755**
GJ 687	0.45	3340.0	–320.6	–1269.5	4.55	9.15	1.698	0.21	0.411	1	0	0.6355	0.3	**0.56**	**0.5**	**0.85**	**0.54**
HD 75289*	1.29	6117.0	–20.5	–227.9	29.14	6.35	0.468	1.55	2.711	1	0	0.999	0.06	**0.54**	**0.633**	**0.838**	**0.694**
HD 42618	1.01	5727.0	197.3	–254.8	24.35	6.839	0.586	0.973	1.718	1	0	0.9795	**0.22**	**0.48**	**0.667**	**0.718**	**0.449**
GJ 832	0.45	3472.0	–45.8	–816.6	4.97	8.66	1.355	0.21	0.408	2	0	0.826	**0.25**	**0.46**	**0.767**	**0.923**	**0.592**
HD 4308	0.93	5686.0	157.5	–741.6	22.03	6.56	0.515	0.827	1.461	1	0	0.998	**0.26**	**0.46**	**0.733**	**0.769**	**0.633**
55 Cnc*	0.91	5196.0	–485.9	–233.7	12.59	5.96	0.391	0.814	1.461	5	0	0.458	0.021	**0.44**	**0.786**	**0.851**	**0.898**
alf Ari	1.5	4553.0	190.73	–145.77	20.21	2.0	0.3	2.275	4.196	1	0	0.5595	0.0	**0.44**	**0.6**	**0.88**	**1.0**
HD 114613	1.27	5641.0	–381.6	46.1	20.29	4.85	0.3	1.546	2.736	1	0	0.905	0.0	**0.42**	**0.567**	**0.588**	**0.98**
Fomalhaut	1.92	8590.0	329.22	–164.22	7.7	1.16	0.3	3.232	5.576	1	0	1.0	0.08	**0.4**	**0.467**	**0.658**	**0.429**
HD 154345	0.71	5468.0	123.2	853.7	18.29	6.76	0.565	0.488	0.868	1	0	0.941	**0.28**	**0.36**	**0.567**	**0.899**	**0.49**
HD 134987	1.1	5736.0	–400.3	–75.2	26.2	6.45	0.49	1.153	2.036	2	0	0.068	0.0	0.34	0.448	0.724	0.837
HD 87883	0.66	4915.0	–64.6	–61.6	18.3	7.55	0.813	0.434	0.788	1	0	0.852	0.18	**0.32**	**0.4**	**0.723**	**0.286**
HD 7924	0.65	5131.0	–34.6	–32.7	17.0	7.185	0.687	0.416	0.75	3	0	0.9915	0.17	**0.28**	**0.464**	**0.871**	**0.469**
HD 164922	0.76	5372.0	389.7	–602.3	22.02	6.99	0.628	0.562	1.003	2	0	0.882	0.149	**0.26**	**0.621**	**0.793**	**0.408**
HD 90156	0.84	5599.0	–39.1	99.1	21.96	6.92	0.608	0.678	1.201	1	0	0.992	0.14	**0.24**	**0.533**	**0.769**	**0.469**
HD 150706	1.17	5961.0	94.9	–87.0	28.29	7.02	0.637	1.287	2.259	1	0	0.7255	0.02	0.22	**0.4**	**0.667**	**0.571**
HD 189733*	0.79	5052.0	–3.3	–250.2	19.78	7.67	0.859	0.618	1.115	1	0	1.0	0.06	0.18	**0.367**	**0.773**	**0.449**
HD 164595	0.99	5790.0	–139.1	173.5	28.28	7.1	0.661	0.931	1.641	1	0	0.9965	0.04	0.18	**0.367**	**0.701**	**0.286**
HD 97658	0.89	5175.0	–107.5	48.7	21.58	7.71	0.875	0.779	1.4	1	0	1.0	0.1	0.16	**0.533**	**0.761**	**0.469**
HD 147379*	0.6	4156.0	–498.0	84.1	10.77	8.896	1.511	0.368	0.693	1	0	0.4805	0.08	0.16	**0.467**	**0.792**	0.24
HD 62509	2.1	4946.0	–625.69	–45.95	10.34	1.14	0.3	4.311	7.819	1	0	0.887	0.0	0.14	0.133	**0.248**	**0.735**
HD 104067	0.62	4937.0	141.9	–423.9	20.38	7.93	0.968	0.383	0.694	1	0	0.7075	0.02	0.12	0.267	**0.538**	0.245
HD 192263	0.66	4976.0	–62.7	261.0	19.65	7.79	0.908	0.433	0.784	1	0	0.906	0.04	0.08	**0.3**	**0.647**	0.184
HD 70642	0.96	5665.0	–202.0	224.8	29.3	7.18	0.685	0.882	1.56	1	0	0.3135	0.0	0.08	0.433	**0.667**	0.224
HD 82943	1.2	6016.0	1.5	–174.7	27.61	6.53	0.508	1.349	2.365	2	0	0.0	0.0	0.0	0.0	0.0	0.0
HD 215152	0.77	4935.0	–154.1	–289.7	21.61	8.11	1.052	0.59	1.071	4	0	0.9925	0.021	0.06	0.179	**0.579**	**0.245**
GJ 674	0.35	3600.0	572.6	–880.3	4.55	9.37	1.879	0.148	0.287	1	0	0.993	0.08	0.06	**0.5**	**0.725**	**0.3**
GJ 849	0.65	3241.0	1132.5	–22.1	8.8	10.37	2.979	0.439	0.863	1	0	0.7645	0.04	0.04	0.067	**0.417**	0.16
HD 176986	0.79	4931.0	–126.9	–235.9	27.81	8.42	1.213	0.621	1.127	2	0	0.994	0.0	0.04	0.069	**0.319**	0.041
GJ 536	0.52	3685.0	–825.4	598.1	10.41	9.72	2.208	0.279	0.538	1	0	0.997	0.02	0.04	0.1	**0.233**	0.08
GJ 96	0.6	3785.0	215.926	41.087	11.94	9.345	1.858	0.371	0.711	1	0	0.7285	0.04	0.04	0.2	**0.467**	0.24
GJ 433	0.59	3461.0	–70.8	–850.7	9.07	9.806	2.297	0.361	0.702	1	0	0.9955	0.04	0.04	**0.333**	**0.508**	0.12
HD 113538	0.58	4462.0	–786.0	–795.6	16.29	9.057	1.627	0.341	0.632	2	0	0.784	0.021	0.04	0.133	**0.35**	0.061
HD 99492*	0.48	4815.0	–728.3	188.5	18.21	7.58	0.824	0.231	0.42	1	0	0.95	0.0	0.04	**0.233**	**0.504**	0.163
HD 46375	0.92	5285.0	111.5	–96.9	29.58	7.912	0.96	0.828	1.482	1	0	0.9975	0.02	0.04	0.167	**0.436**	**0.224**
GJ 625	0.3	3499.0	432.1	–171.7	6.47	10.1	2.63	0.124	0.242	1	0	0.978	0.0	0.02	0.133	**0.258**	0.04
GJ 581	0.31	3480.0	–1221.5	–97.1	6.3	10.56	3.251	0.129	0.251	3	0	0.9775	0.0	0.02	0.103	**0.31**	0.0
Wolf 1061	0.29	3342.0	–94.0	–1183.8	4.31	10.03	2.547	0.12	0.235	3	0	0.859	0.0	0.02	**0.345**	**0.741**	0.0
GJ 667 C	0.33	3350.0	1131.6	–215.5	7.25	10.22	2.78	0.139	0.272	5	2	—-	0.0	0.02	0.036	0.132	0.041
GJ 328	0.69	3900.0	44.7	–1046.0	20.54	9.97	2.477	0.49	0.933	1	0	0.825	0.0	0.02	0.0	0.043	0.02
GJ 649	0.54	3700.0	–115.5	–507.9	10.38	9.69	2.178	0.301	0.579	1	0	0.788	0.04	0.02	0.2	**0.358**	0.1
HD 156668	0.77	4850.0	–72.6	216.8	24.35	8.42	1.213	0.592	1.078	1	0	0.996	0.0	0.02	**0.267**	**0.308**	0.041
Ross 458	0.49	3621.0	–632.2	–36.0	11.51	9.72	2.208	0.248	0.479	1	0	0.7825	0.02	0.02	0.133	**0.275**	0.0

Table 1 *Continued.*

Star Name	Mass ($M_\odot$)	$T_{\rm eff}$ (K)	μ_α (mas yr^{-1})	μ_δ (mas yr^{-1})	d (pc)	V (mag)	σ (μas)	ihz (AU)	ohz (AU)	$N_{\rm num}$	$N_{\rm habi}$	$P_{\rm habi}$	$P_{\rm HP4}$				
													$P_{\rm D3}$	$P_{\rm D5/F10}$	$P_{\rm F20}$	$P_{\rm F50}$	$P_{\rm D8}$
GJ 1148	0.35	3264.0	–575.7	–90.0	11.02	11.92	6.081	0.149	0.293	2	1	—	0.146	0.02	0.067	0.034	0.041
HD 93083	0.7	4995.0	–92.7	–152.2	28.54	8.3	1.148	0.486	0.88	1	0	0.017	0.0	0.02	0.067	0.308	0.122
BD-06 1339	0.7	4324.0	–1.0	–346.7	20.28	9.7	2.188	0.499	0.931	2	0	0.3835	0.0	0.02	0.0	0.188	0.061
GJ 3942	0.63	3867.0	203.9	62.0	16.94	10.25	2.818	0.409	0.78	1	0	0.9945	0.0	0.0	0.033	0.067	0.0
Ross 128	0.17	3192.0	607.7	–1223.3	3.37	11.15	4.266	0.065	0.128	1	0	0.803	0.0	0.0	0.067	**0.408**	0.0
Kapteyn	0.28	3550.0	6491.5	–5709.2	3.93	8.845	1.476	0.115	0.223	1	0	0.753	0.0	0.0	**0.467**	**0.825**	0.0
HD 285968	0.45	3679.0	656.4	–1116.5	9.47	10.038	2.556	0.209	0.403	1	0	0.994	0.02	0.0	0.067	**0.25**	0.02
GJ 436	0.47	3318.0	895.0	–814.0	9.76	10.67	3.42	0.229	0.449	1	0	1.0	0.0	0.0	0.033	0.133	0.02
HD 85512	0.43	4300.0	461.4	–472.0	11.28	7.67	0.859	0.189	0.352	1	1	—	0.0	0.0	0.0	0.042	0.0
GJ 273	0.29	3382.0	572.51	–3693.51	3.8	9.872	2.368	0.12	0.234	2	0	0.852	0.0	0.0	**0.379**	**0.802**	0.061
HIP 57274	0.29	4510.0	–27.1	–381.7	25.88	8.98	1.57	0.117	0.216	3	1	—	0.0	0.0	0.036	0.0	0.0
HD 181433	0.63	4918.0	–230.9	235.8	26.9	8.4	1.202	0.395	0.718	3	0	0.801	0.0	0.0	0.036	0.207	0.041
GJ 9827	0.61	4269.0	376.0	216.1	29.69	10.25	2.818	0.38	0.71	3	0	1.0	0.0	0.0	0.0	0.009	0.0
YZ Cet	0.13	3056.0	1208.53	640.73	3.6	12.074	6.528	0.048	0.095	3	0	0.9845	0.0	0.0	0.0	0.121	0.0
GJ 876	0.32	3129.0	958.0	–673.6	4.68	10.191	2.743	0.135	0.266	4	1	—	0.0	0.0	0.0	**0.466**	0.0
HD 102195	0.76	5301.0	–188.7	–113.4	29.36	8.062	1.029	0.564	1.01	1	0	0.988	0.0	0.0	0.067	**0.274**	0.061
51 Eri	1.75	7331.0	44.4	–63.8	29.78	5.23	0.3	2.676	4.614	1	0	0.8745	0.0	0.0	0.0	0.034	**0.286**
GJ 3779	0.27	3324.0	–615.951	–865.128	13.75	12.96	9.817	0.11	0.216	1	0	0.994	0.0	0.0	0.0	0.0	0.0
gam Cep*	1.4	4800.0	–63.0	171.5	13.54	3.21	0.3	1.962	3.581	1	1	—	0.0	0.0	0.0	0.0	0.0
GJ 179	0.36	3370.0	153.4	–306.1	12.36	12.0	6.31	0.154	0.3	1	0	0.9105	0.0	0.0	0.0	0.0	0.0
GJ 1214	0.15	3026.0	580.4	–749.6	14.65	15.1	26.303	0.056	0.112	1	0	1.0	0.0	0.0	0.0	0.0	0.0
WD 0806-661	0.62	10205.0	335.5	–288.9	19.26	13.71	13.868	0.52	0.928	1	0	0.8465	0.0	0.0	0.0	0.0	0.0
GJ 1265	0.18	3236.0	856.89	–306.305	10.26	13.57	13.002	0.069	0.136	1	0	0.9815	0.0	0.0	0.0	0.0	0.0
HD 147513	1.11	5883.0	74.1	3.7	12.91	5.39	0.301	1.164	2.047	1	1	—	0.0	0.0	0.0	0.0	0.0
TRAPPIST-1	0.08	2559.0	930.9	–479.4	12.43	18.8	144.544	0.028	0.056	7	3	—	0.0	0.0	0.0	0.0	0.0
bet Pic	1.76	8052.0	2.5	82.6	19.75	3.85	0.3	2.674	4.604	1	0	0.0	0.0	0.0	0.0	0.0	0.0
GJ 1132	0.18	3270.0	–1054.0	414.3	12.62	13.49	12.531	0.069	0.136	2	0	0.8845	0.0	0.0	0.0	0.0	0.0
GJ 317	0.42	3510.0	–461.2	805.6	15.2	11.97	6.223	0.183	0.356	2	0	0.13	0.0	0.0	0.0	0.0	0.0
HD 128311	0.83	4965.0	204.4	–250.4	16.34	7.51	0.798	0.685	1.241	2	1	—	0.0	0.0	0.0	0.0	0.0
GJ 3998	0.5	3722.0	–137.3	–347.3	18.16	10.83	3.681	0.258	0.496	2	0	0.9945	0.0	0.0	0.0	0.0	0.0
HD 114783	0.85	5135.0	–138.4	10.2	21.08	7.55	0.813	0.712	1.282	2	1	—	0.0	0.0	0.0	0.0	0.0
ups And*	1.3	6213.0	–172.2	–382.9	13.41	4.1	0.3	1.564	2.732	3	1	—	0.0	0.0	0.0	0.0	0.0
GJ 163	0.4	3500.0	1046.1	584.1	15.14	11.81	5.781	0.173	0.336	3	0	0.881	0.0	0.0	0.0	0.0	0.0
HD 20794	0.7	5401.0	3033.7	730.8	6.0	4.27	0.3	0.476	0.849	4	1	—	0.0	0.0	0.0	0.0	0.0
HD 160691	1.08	5807.0	–15.3	–190.9	15.61	5.15	0.3	1.107	1.95	4	1	—	0.0	0.0	0.0	0.0	0.0
GJ 676 A*	0.73	3734.0	–257.9	–184.5	16.03	9.58	2.07	0.55	1.056	4	0	0.0	0.0	0.0	0.0	0.0	0.0
GJ 3293	0.42	3466.0	–81.4	–485.5	20.2	11.962	6.2	0.183	0.357	4	1	—	0.0	0.0	0.0	0.009	0.0
HD 40307	0.77	4956.0	–52.4	–60.2	12.94	7.17	0.682	0.589	1.069	5	1	—	0.0	0.0	0.0	0.0	0.0
LHS 1140	0.18	3216.0	317.6	–596.6	14.99	14.18	17.219	0.069	0.137	2	1	—	0.0	0.0	0.0	0.0	0.0
GJ 3323	0.16	3159.0	–551.7	–533.9	5.38	12.22	6.982	0.061	0.12	2	0	0.3125	0.0	0.0	0.0	0.026	0.0
GJ 3634	0.45	3313.0	–566.9	–91.4	20.39	11.93	6.109	0.21	0.412	1	0	1.0	0.0	0.0	0.0	0.0	0.0
HD 128356	0.65	4875.0	–19.3	–137.9	26.03	8.29	1.143	0.422	0.767	1	0	0.0	0.0	0.0	0.0	0.0	0.0
HD 210277	1.01	5538.0	85.5	–450.5	21.31	14.4	19.055	0.984	1.746	1	1	—	0.0	0.0	0.0	0.0	0.0
16 Cyg B	1.08	5750.0	–134.8	–162.5	21.15	6.25	0.447	1.111	1.96	1	1	—	0.0	0.0	0.0	0.0	0.0
GJ 3341	0.47	3526.0	494.2	249.8	23.64	12.08	6.546	0.229	0.444	1	0	0.9955	0.0	0.0	0.0	0.0	0.0
HIP 12961	0.69	3901.0	294.9	141.0	23.39	10.24	2.805	0.49	0.933	1	0	0.856	0.0	0.0	0.0	0.017	0.0
HIP 70849*	0.63	4105.0	–44.0	–201.8	24.07	10.36	2.965	0.407	0.767	1	0	0.7025	0.0	0.0	0.067	0.026	0.0
GJ 3470	0.51	3652.0	–185.7	–57.3	29.45	12.33	7.345	0.269	0.518	1	0	1.0	0.0	0.0	0.0	0.0	0.0
BD-11 4672	0.57	4475.0	–288.6	–235.6	27.19	9.99	2.5	0.329	0.61	1	0	0.927	0.0	0.0	0.0	0.009	0.0
HD 114386	0.6	4836.0	–137.1	–324.9	27.95	8.73	1.4	0.36	0.656	1	0	0.6655	0.0	0.0	0.033	0.085	0.0
HD 125595	0.29	4691.0	–561.6	–68.5	28.22	9.03	1.607	0.116	0.213	1	0	0.8855	0.0	0.0	0.0	0.068	0.0
HD 204941	0.58	5026.0	–279.1	–124.2	28.74	8.45	1.23	0.333	0.603	1	0	0.9725	0.0	0.0	0.067	0.077	0.02
HD 218566	0.76	4730.0	631.5	–97.2	28.85	8.628	1.335	0.58	1.061	1	1	—	0.0	0.0	0.0	0.0	0.0
Proxima Cen	0.12	3050.0	–3775.64	768.16	1.29	11.11	4.188	0.044	0.087	1	1	—	0.0	0.0	0.0	0.0	0.0
HSV 1 256	0.07	2620.0	–277.0	–189.0	12.7	17.759	89.495	0.024	0.048	1	0	0.0	0.0	0.0	0.0	0.0	0.0
alf Tau	1.13	4055.0	62.78	–189.36	20.43	0.85	0.3	1.31	2.475	1	1	—	0.0	0.0	0.0	0.0	0.0
K2-129	0.36	3459.09	51.4	–312.1	27.82	13.63	13.366	0.154	0.299	1	0	1.0	0.0	0.0	0.0	0.0	0.0
70 Vir	1.09	5495.0	–235.6	–576.3	17.91	4.97	0.3	1.148	2.042	1	0	0.0	0.0	0.0	0.0	0.0	0.0
HD 39091	1.09	6037.0	311.2	1048.8	18.28	5.67	0.342	1.112	1.948	2	0	0.0	0.0	0.0	0.0	0.0	0.0
HD 10647	1.11	6218.0	165.8	–105.5	17.34	5.52	0.319	1.14	1.991	1	0	0.0	0.0	0.0	0.0	0.0	0.0
HD 27442*	1.23	4846.0	–48.3	–167.8	18.28	4.44	0.3	1.512	2.753	1	0	0.0	0.0	0.0	0.0	0.0	0.0
HD 219077	1.05	5362.0	478.2	–424.1	29.21	6.12	0.421	1.074	1.917	1	0	0.0	0.0	0.0	0.0	0.0	0.0
HD 33564	1.25	6250.0	–78.4	162.1	20.97	5.08	0.3	1.443	2.518	1	0	0.0	0.0	0.0	0.0	0.0	0.0
GJ 3021*	0.9	5540.0	433.9	–56.3	17.56	6.59	0.522	0.781	1.386	1	0	0.0	0.0	0.0	0.0	0.0	0.0
14 Her	0.9	5338.0	132.0	–296.5	17.94	6.61	0.527	0.79	1.412	1	0	0.0	0.0	0.0	0.0	0.0	0.0
HD 30562	1.12	5882.0	311.4	–249.1	26.18	5.78	0.36	1.185	2.084	1	0	0.0	0.0	0.0	0.0	0.0	0.0
HD 60532	1.5	6245.0	–39.8	46.5	25.99	4.44	0.3	2.079	3.628	2	0	0.0	0.0	0.0	0.0	0.0	0.0
HD 216437	1.06	5887.0	–43.5	73.0	26.71	6.05	0.407	1.061	1.866	1	0	0.0	0.0	0.0	0.0	0.0	0.0

Table 1 *Continued.*

Star Name	Mass ($M_\odot$)	$T_{\rm eff}$ (K)	μ_α (mas yr^{-1})	μ_δ (mas yr^{-1})	d (pc)	V (mag)	σ (μas)	ihz (AU)	ohz (AU)	$N_{\rm num}$	$N_{\rm habi}$	$P_{\rm habi}$	$P_{\rm HP4}$				
													$P_{\rm D3}$	$P_{\rm D5/F10}$	$P_{\rm F20}$	$P_{\rm F50}$	$P_{\rm D8}$
HD 142*	1.23	6245.0	575.0	–40.7	26.21	5.7	0.347	1.398	2.439	2	0	0.0	0.0	0.0	0.0	0.0	0.0
47 UMa	1.03	5892.0	–317.6	55.0	13.8	5.05	0.3	1.002	1.761	3	0	0.0	0.0	0.0	0.0	0.0	0.0
7 CMa	1.52	4792.0	62.0	–72.8	19.82	3.92	0.3	2.314	4.224	1	0	0.0	0.0	0.0	0.0	0.0	0.0
HD 111232	0.84	5512.0	27.3	112.4	28.98	7.59	0.828	0.681	1.211	1	0	0.0	0.0	0.0	0.0	0.0	0.0
HIP 79431	0.42	3368.0	35.7	–214.0	14.54	11.34	4.656	0.183	0.359	1	0	0.0	0.0	0.0	0.0	0.0	0.0

able to achieve the highest precision of 0.3 μas. We list the estimates of precision of astrometric measurements of every stars in our sample, as well as their V-band magnitude in Table 1.

2.2 Injecting Earth-like Planets in HZ

One of the scientific goals of HEPS is to find HEs around other stars. However, most of the selected systems in our sample lack planets in their HZs. To check whether an HE is detectable by HEPS, we first need to calculate the HZ of each system before injecting an HE to the system.

The habitable region around each star varies based on the stellar parameters. We calculate the HZ around each star using the method described in Kopparapu et al. (2013), where stellar spectral energy and planetary atmosphere mode are both considered. The Runaway Greenhouse Effect and the Moist Greenhouse Effect are selected in our work to calculate the inner boundary and the outer boundary of the HZs, respectively (for more details, we refer the readers to eq. 2 and table 3 in Kopparapu et al. 2013). The stellar luminosity data is not complete for the stars in our sample, we therefore use the empirical mass-luminosity relation to calculate them. The location of the inner boundary and the outer boundary of the HZ of each star is listed in Table 1. We note that the HZ mode in Kopparapu et al. (2013) is for main-sequence stars with $T_{\rm eff}$ between 2600 K and 7200 K, in which case six of the stars in our sample exceed this range, which may lead to slightly inaccurate HZ ranges.

The range of HZ is also affected by whether or not it is of a binary system (Eggl et al. 2012; Haghighipour & Kaltenegger 2013). All of the binary systems in our sample are of large separations, which makes the flux from the companion stars negligible. The influence from the companion stars to the HZs of the planet-harboring stars in binary systems is therefore not taken into consideration. Figure 2 shows the HZs of the selected 140 planetary systems, sorted by stellar mass in ascending order. Three stars, Proxima Centauri, GJ 3293 and eps Eri, are labeled to show both their HZs and the locations of the detected planets.

For systems without known planets in their HZs, we randomly inject an HE in each system. Before carrying out further astrometric simulations, it is necessary to ensure the stability of the injected systems. We briefly describe our method here.

Most of the detected planets in our sample are either discovered by RV or have RV follow-up observations, which only gives the minimum mass of any detected planet because of the mass-inclination degeneracy, which is in the form of $M_{\rm RV} = M_{\rm p} \sin i$, where $M_{\rm RV}$ is the measured mass from RV observations and i is the inclination of the planet. Assuming that all of the planets in our sample are of planetary mass and a strong coplanarity, the lower limit of inclination is therefore constrained by the largest minimum mass of the system. However, the upper limit of the mass of a planet, which is also the lower limit of the mass of a brown dwarf is still debatable. In our work, we adopt the mass of the imaging planet HR 2562 b (Konopacky et al. 2016), 20.3 $M_{\rm Jupiter}$, as the upper limit. The planet masses used in stability tests are then generated by combining the minimum masses with a uniform distribution of inclinations in the range of $[\arcsin \frac{M_{\rm RV}}{20.3 M_{\rm Jupiter}}, 90]^\circ$. For several planets with masses measured using other techniques, such as transit timing variations or direct imaging, planet masses are directly adopted from the NASA Exoplanet Archive. The eccentricities, e, the longitudes of ascending node, Ω, and the arguments of periapsis, ω, of the planets in our sample, if available, are directly adopted from the Exoplanet Archive; if not, then they are set as 0 or randomly chosen from a uniform distribution between 0° and 360°, respectively.

A 10 $M_\oplus$ planet is then injected to the HZ of such systems. The probability of such a system being stable, $P_{\rm hab}$, is defined in the form of

$$P_{\rm hab} = N_{\rm stable}/N_{\rm sim}, \tag{3}$$

where $N_{\rm sim}$ is the number of simulations and $N_{\rm stable}$ is the number of stable systems. $P_{\rm hab}$ is calculated by computing the mutual Hill Radius for 100 times, where the system is considered to be stable when the planet separation is larger than 10 times their mutual Hill Radius (Chambers et al. 1996).

The probabilities of different systems with stable injected HEs are listed in Table 1. We note that $P_{\rm hab}$ for systems with known planets in their HZs is always 1.

2.3 Astrometry Simulation

The astrometric signals of the motions of the host stars of the planetary systems on the celestial sphere include the proper motions, the annual parallaxes, the annual aberrations, and the gravitational tug caused the orbital motions of the planets. The right ascension, α, and declination, δ, of a host star can be expressed as:

$$\begin{aligned}\alpha_t =&\alpha_0 + \mu_\alpha^* t \\ &+ \left(\mu_\alpha^* \mu_\delta \tan\delta - \mu_\alpha^* \pi V_{\mathrm{r}}\right) t^2 \\ &+ \pi\left(-y\cos\alpha + x\sin\alpha\right)\sec\delta \\ &- \frac{1}{\mathrm{c}}\left(\dot{x}\cos\alpha\sin\delta - \dot{y}\cos\alpha\sec\delta\right),\end{aligned} \tag{4}$$

$$\begin{aligned}\delta_t =&\delta_0 + \mu_\delta t - \left(\frac{1}{2}\mu_\alpha^{*\,2}\sin\delta\cos\delta + \mu_\delta \pi V_{\mathrm{r}}\right) t^2 \\ &+ \pi\left(x\cos\alpha\sin\delta + y\sin\alpha\cos\delta - z\cos\delta\right) \\ &- \frac{1}{\mathrm{c}}\left(\dot{x}\cos\alpha\sin\delta + \dot{y}\sin\alpha\sin\delta - \dot{z}\cos\delta\right).\end{aligned} \tag{5}$$

In Equations (4) and (5), α_0 and δ_0 are the initial positions ($t = 0$) of the host star, and μ_α^* and μ_δ are the stellar proper motions along the directions of RA and DEC, respectively. The third terms are the accelerations of the stellar proper motions, which are related to the stellar parallaxes, π, and the radial velocities, V_r. The fourth and the fifth terms are the stellar annual parallaxes and the annual aberrations, respectively, which can be calculated assuming the accurate positions (x, y, z) and velocities $(\dot{x}, \dot{y}, \dot{z})$ of the spacecraft are known at any observing time.

Our mode can be simplified without losing significant accuracy, in which case we omit the accelerations of the proper motions, the parameters of annual parallax and the annual aberration. The motions along the directions of RA and DEC can be projected onto X-Y plane, which can be expressed as:

$$X = X_0 + V_{\mathrm{x}}(t - t_0) + P_{\mathrm{x}}/d + \delta_{\mathrm{x}} + \sigma_{\mathrm{x}}, \tag{6}$$

$$Y = Y_0 + V_{\mathrm{y}}(t - t_0) + P_{\mathrm{y}}/d + \delta_{\mathrm{y}} + \sigma_{\mathrm{y}}, \tag{7}$$

where X_0 and Y_0 are the initial positions of the star, V_{x} and V_{y} are the proper motions of the stars, t_0 is the initial time, P_{x} and P_{y} are the parameters of the annual parallaxes, δ_{x} and δ_{y} are the motions caused by the planets, which is calculated using the RKF78 method (Fehlberg E. 1968), and σ_{x} and σ_{y} are the random white noise added to resemble the real observing data according to Equation (2).

2.4 Fitting Procedures of the Simulation Data

To fit for planetary and stellar parameters, we adopt the Levenberg-Marquardt method (Marquardt. 1963), where the Monte Carlo method is also applied to disturb the initial parameters to avoid falling into local minimum. Planet-planet interaction is also neglected during the fitting process because the time span of the simulated data is very short (less than 8 years), in which case the orbital elements are nearly unchanged. We refer the readers to Yu et al. (2019) for more information on the 4-step fitting process, with the only difference being Step 2, where precisely-measured periods are used as the initial values and a 5% interval is applied when fitted. This modification is to avoid the under-sampling problem, where the periods of close-in planets can be hardly fitted if the cadence of HEPS is larger than half of the period. Other parameters, such as e and ω, have large measurement uncertainties, therefore we fit these parameters with no constraint.

To demonstrate the impact of the under-sampling problem, we use the Proxima Centauri (hereafter PC) system as an example, where the host star is only 0.12 $M_\odot$ and the surface temperature is only 3050 K. PC b has a semi-major axis of 0.0485 AU (11.262 days), which is well within the range of the HZ of PC, which is from 0.0436 AU (9.599 days) to 0.0865 AU (26.82 days). The minimum mass of PC b we adopt here is 1.27 $M_\oplus$ and the real mass is related to the inclination of the planet. Here the inclination is set as $7.7249°$, which leads to the mass of PC b 9.45 $M_\oplus$.We set the duration of the observation to be 5 years (year $=$ 5). Simulation 1 contains the results of 50 measurements with even cadence per year (f $=$ 50), and Simulation 2 contains the results of 100 measurements (f $=$ 100) under the same conditions. During the fitting process, the initial period of the planet is set as 0.0308 yr and is not constrained. The values of the simulated planetary orbital elements and our fitting results of Simulation 1 and 2 are listed in Table 2. The periodograms of the directions of X and Y in Simulation 1 and 2 are plotted in the right panels of Figure 3 and Figure 4, respectively, while the left panels of Figure 3 and Figure 4 show the phase-folded data. In Simulation 1, it is almost impossible to retrieve the period of PC b because the sampling cadence is larger than half of its period, ~ 0.0154 yr. In Simulation 2, however, the cadence is smaller than ~ 0.0154 yr, making the retrieved parameters much more accurate than those of Simulation 1, especially the values of mass and period.

3 DETECTION PROBABILITY OF THE PLANETS IN HZ

3.1 Simulation Results of the Selected Sample

The typical observation mode of HEPS is observing every target 10 times per year during its 5-year mission time, making the sampling cadence about 36.5 days. The HZ around different planet hosts, however, varies significant-

Table 2 Real and Fitted Parameters of Proxima Centauri b in Simulations 1 and 2

Name	$M_{\rm p}(M_\oplus)$	Period (yr)	a (AU)	ecc	inc (deg)	Ω (deg)	ω+ M_0 (deg)
b	9.45	0.0308	0.0485	0.35	7.7249	310.0	15.47
Fitted result for Simulation 1							
b	6.75	0.057	0.073	0.386	24.80	55.87	45.32
Fitted result for Simulation 2							
b	9.75	0.0308	0.0485	0.329	12.32	306.78	14.01

Table 3 16 Prior Systems with High $P_{\rm t}$

Name	Mass	Distance	$P_{\rm habi}$	$P_{\rm t}$	$P_{\rm HP4}$ in different modes				
	($M_\odot$)	(pc)	.		f10	f20	f50	D8	D3
HN Peg	1.1	18.13	1.0	1.0	1.0	1.0	1.0	0.98	0.88
HD 219134	0.81	6.53	1.0	0.98	0.98	1.0	0.991	0.98	0.809
61 Vir	0.94	8.51	0.97	0.931	0.96	0.966	0.991	1.0	0.553
51 Peg	1.12	15.47	0.996	0.896	0.9	0.833	0.967	0.94	0.76
HD 3651	0.88	11.14	0.968	0.871	0.9	0.9	0.95	0.92	0.8
tau Boo	1.34	15.66	1.0	0.84	0.84	0.667	0.8	0.72	0.32
HD 26965	0.78	5.04	0.998	0.838	0.84	0.967	0.975	0.94	0.76
HD 177565	1.0	16.93	0.999	0.799	0.8	0.867	0.8	0.7	0.52
GJ 86	0.93	10.79	0.887	0.798	0.9	0.867	0.9	0.92	0.8
GJ 504	1.22	17.54	0.991	0.793	0.8	0.833	0.917	0.92	0.1
HD 102365	0.85	9.29	0.944	0.736	0.78	1.0	0.975	0.9	0.88
HD 1461	1.02	23.47	1.0	0.66	0.66	0.862	0.914	0.816	0.277
HD 16417	1.2	25.41	1.0	0.6	0.6	0.667	0.889	0.755	0.1
eps Eri	0.83	3.2	0.602	0.566	0.94	0.933	1.0	0.98	0.82
rho CrB	0.89	17.48	0.9	0.558	0.62	0.967	0.949	0.653	0.354
HD 114613	1.27	20.29	0.904	0.38	0.42	0.567	0.588	0.98	0.0

ly based on the spectral types of the host stars, in which case, for M dwarfs similar to PC, the inner boundaries of their HZs are less than several tens of days, while for stars more massive, like β Pictoris, the inner boundaries of their HZs are better expressed in unit of year. We therefore test two types of observation modes, mainly a change from the typical mode in either sampling cadence or total observation time of a single target, in our simulations to see the goodness of the fits of the simulated signals.

Type 1: Changing the observation cadence. 10, 20 and 50 measurements per year with even interval, which are represented as Mode f10, f20 and f50, respectively, are tested.

Type 2: Changing the total observation time of a single target. 3, 5 and 8 years, which are represented as Mode D3, D5, D8, respectively, are tested.

We note that Modes f10 and D5 are the same as the typical observation mode, which is only tested once. For all other different modes, we generate the astrometric signals using the method described in Section 2 and check the goodness of fit by comparing the fitted parameters with their initial values. In total, 50 cases are simulated for each mode. Since some planetary parameters are randomly set in our simulation, the fitting results may deviate from each other in different simulations for the same planetary system. We define the probability of detection of the HEs, $P_{\rm HP}$, as

$$P_{\rm HPi} = \frac{N_{\rm cri}}{50}\,, \tag{8}$$

where i indicates the number of satisfied criteria, and $N_{\rm cri}$ is the number of cases satisfying different criteria, which represents the goodness of fit of the fitted parameters. The criteria used in this paper are the same with those in Yu et al. (2019), with the only difference being the criterion for planet mass, which now requires the relative error of mass to be less than 5 percent. When calculating $P_{\rm HP4}$, $N_{\rm cri}$ is the number of systems satisfying all four criteria listed in Yu et al. (2019), which include constraints on the fitting results of planetary masses and orbital elements, such as the semi-major axis of the fitted planet must be within range of the HZ of the system, the mass of the fitted planet must be Earth-like, and the uncertainties of eccentricity and inclination are must be smaller than 0.1 and 5°, respectively. We note that for systems with known giant planets in their HZs, $P_{\rm HP4}$ is also calculated for them.

A stable system is the pre-requisition for detecting an HE, therefore the true probability of detection of an HE is the combination of $P_{\rm hab}$ (Eq. (3)) and $P_{\rm HP4}$. The true probability of detecting an HE, $P_{\rm t}$, can then be expressed as

$$P_{\rm t} = P_{\rm hab} * P_{\rm HP4}\,. \tag{9}$$

For each observation mode, we sort the planet hosts by $P_{\rm t}$ in descending order and obtain the top 10 systems. We list them in Table 3 if the system is one of the top 10

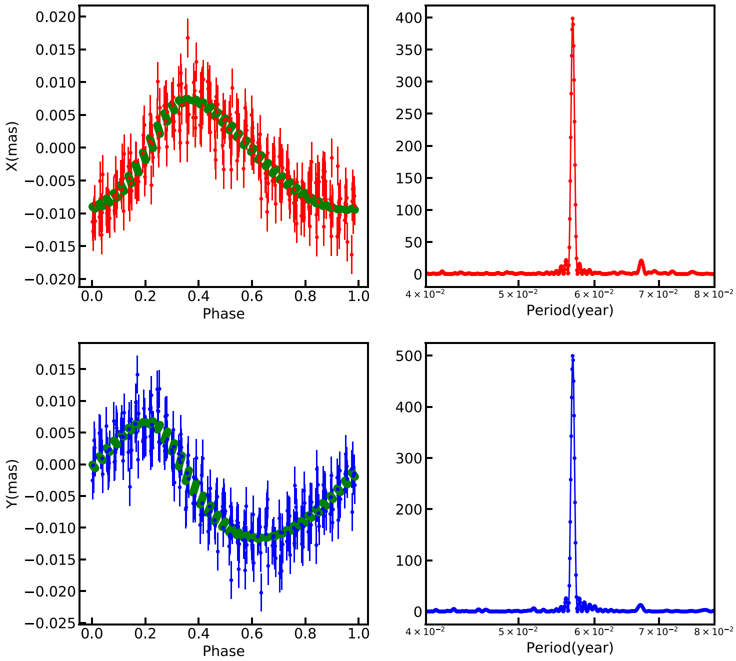

Fig. 3 Fitting results of Simulation 1, i.e., 50 measurements per year with even interval, during the 5 year observations. The left and right panels show the signals and periodograms of movements of Proxima in the X and Y direction due to Proxima b, respectively.

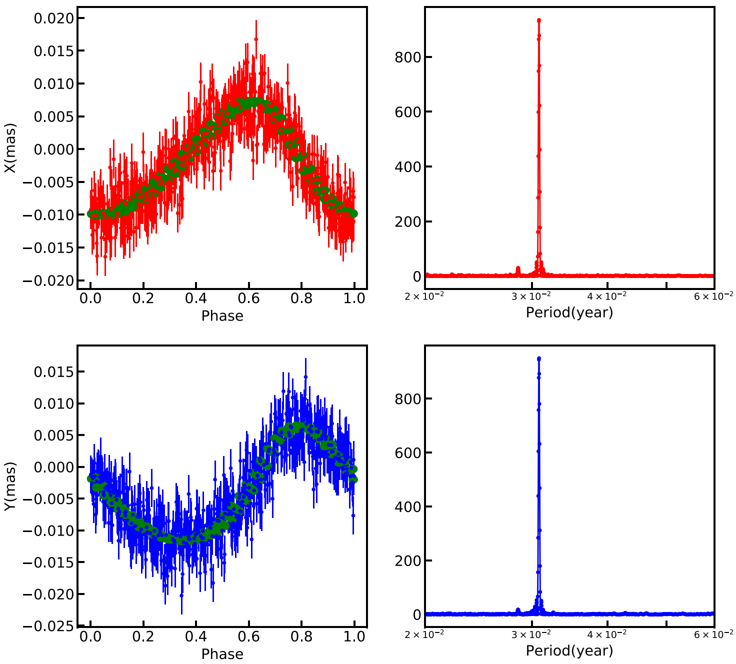

Fig. 4 Similar to Fig. 3, the fitting results of Simulation 2, i.e., 100 measurements per year with even interval, during the 5 year observations.

in at least one of the five modes. Duplicities are excluded. In Table 3, we only show the $P_{\rm t}$s of the typical mode for simplicity, while $P_{\rm HP4}$s of different modes are listed. In most cases, it is not unexpected that $P_{\rm HP4}$ increases with the lifetime of HEPS or the number of measurements per year.

The detection probabilities of all 140 systems are listed in Table 1, sorted by $P_{\rm HP4}$ of Mode f10 in descending order. Figure 5 shows the histograms for $P_{\rm HP4}$ of Mode f20 against the stellar mass, distance, number of known planets, and periods of the planets in HZ. In Panel a, although most stars have masses between 0.25 and 1.25 $M_\odot$, we find stars with masses between 0.75 and 1.5 $M_\odot$ have the largest detection probabilities, $\sim$50%. Panel b shows that $P_{\rm HP4}$ decrease significantly with increasing distance, and a gap near 15 pc is present, due to lower SNRs. The planet hosts within $15 - 18$ pc have the largest average $P_{\rm HP4}$, which is larger than 70%. In Panel c, systems with fewer planets have larger $P_{\rm HP4}$, which is consistent with our results of Paper I. For several extreme systems with more than four planets, the probability has a larger uncertainty statistically. In Panel d, planets in HZ with a period of 1 to 5 years, which make up more than 70% of all planets in our sample, have a $P_{\rm HP4}$ larger than 50%, indicating that f20 is a suitable mode to detect planets around most stars in our sample.

3.2 Empirical Estimation of $P_{\rm HP4}$

As seen in Section 3.1, the sampling cadence and observation time on single targets significantly influence $P_{\rm HP4}$. The left panel of Figure 6 shows that the SNR still plays an important role as it does in Yu et al. (2019) in determining $P_{\rm HP4}$, because the blue line well defines the upper limit of the distribution of the real data. Points of real data not following the theoretical line are possibly the results of additional uncertainties from the fitting of other planets, which is different from Yu et al. (2019), where only single-planet systems are considered. $P_{\rm HP4}$ of five different modes are plotted in the right panel of Figure 6, which also shows that $P_{\rm HP4}$ benefits greatly from more measurements and longer coverage of single targets.

To analyze the influence on $P_{\rm HP4}$ due to different factors, we define $f(\rm Freq, Dur)$ as the influence of the sampling cadence and total coverage time, in which case $P_{\rm HP4}$ can be rewritten as the product of three factors, in the form of

$$P_{\rm HP4} = P_{\rm SNR} * P_{\rm S} * f(\rm Freq, Dur)\,, \qquad (10)$$

where $P_{\rm SNR}$ and $P_{\rm S}$ are the influence due to the SNR of the planet in HZ and the fitting residuals of other planets, which are defined in equations (8), (9) and (10) in Yu et al. (2019), respectively. As mentioned earlier, an increase in the total coverage time or the sampling frequency will result in more data points in one phase after phase folding, after which the SNR can be improved by binning the folded data points, resulting in a higher detection probability. The influence of the two factors, when staying unchanged, also varies with the period of the planet in HZ. To exclude this variation, we define two parameters, D and F as

$$D = \rm Dur/Period\,, \quad F = Period * Freq\,, \qquad (11)$$

where Period is the period of the planet in HZ, Dur is the total coverage time, and Freq is the sampling frequency. $f(F, D)$ now represents the influence of the two factors independent from the period of the planet in HZ. To investigate how F and D influence the detecting probability, it is necessary to exclude the influence of SNR ($P_{\rm SNR}$) and other planets ($P_{\rm S}$) from $P_{\rm HP4}$. In Yu et al. (2019), we have obtained the expression of $P_{\rm SNR}$ and $P_{\rm S}$, we therefore define another probability P_3 as follows:

$$P_3 = P_{\rm HP4}/(P_{\rm SNR} \times P_{\rm S}) = f(F, D)\,. \qquad (12)$$

Note that $P_{\rm SNR}$ and $P_{\rm S}$ are obtained in Mode f10 and the HZs around solar-like star are adopted from paper I. In this work, more measurements are also able to improve the SNR of the data, therefore $P_{\rm F}$ and $P_{\rm D}$ with larger D or F may be larger than one, and enhance the total probability.

Using simulated data, the dependency between P_3 and F and D can be investigated. To constrain the expression of $f(D, F)$, we choose a subset from the simulated sample to see if D and F can influence $f(D, F)$ independently. The left panel of Figure 7 shows the influence of D on systems with $F > 15$. We only plot systems with D within the range of 0.5 to 16. Beyond this range, few systems are found in our simulations, we therefore exclude them to reduce the influence of the statistical uncertainty. $P_D = f(D, F > 15)$ can be expressed as,

$$P_D = 0.03767D^2 + 0.6357D - 0.3263, \text{when } 1 \leq D \leq 16. \qquad (13)$$

Since most of the planet periods in HZs in our sample are larger than 12 days (see Fig. 2), the minimum cadence should be 6 days to ensure the retrieval of the correct period, based on the Nyquist sampling theorem. Systems with F from 2 to 60 are thus selected to test the dependency of P_3 on F. We also select systems with $D > 1$, which are the majority in our simulations. Since D influences P_3 significantly according to Equation (13), we define another factor $P_4 = P_3/P_{\rm D}$ and estimate P_4 for each system with different D to exclude the influence of D. The right panel of Figure 7 shows the results of P_4 with different F. The correlation between P_4 and F is linear if F is smaller than 60. The fitting results are good enough considering the uncertainty of P_4, which is in the form of

$$P_4 = 0.03407F - 0.06605, \quad 2 \leq F \leq 60. \qquad (14)$$

Note that Equations (13) and (14) are only suitable for estimating the expression of $f(D, F)$, which is $f(D, F) = g(D) \times h(F)$, where $g(D)$ is linear and $h(F)$ is quadratic. We use expression to fit all data within the range of $2 \leq F \leq 60$ and $1 \leq D \leq 16$ and obtain the empirical estimation of $f(D, F)$ as follows:

$$P_3 = (0.040F - 0.021) \times (0.058D^2 + 0.340D - 0.216). \qquad (15)$$

We plot $f(D, F)$ in the left panel of Figure 8, and the differences between the empirical estimation and the simulated values of P_3 are shown in the right panel. In the

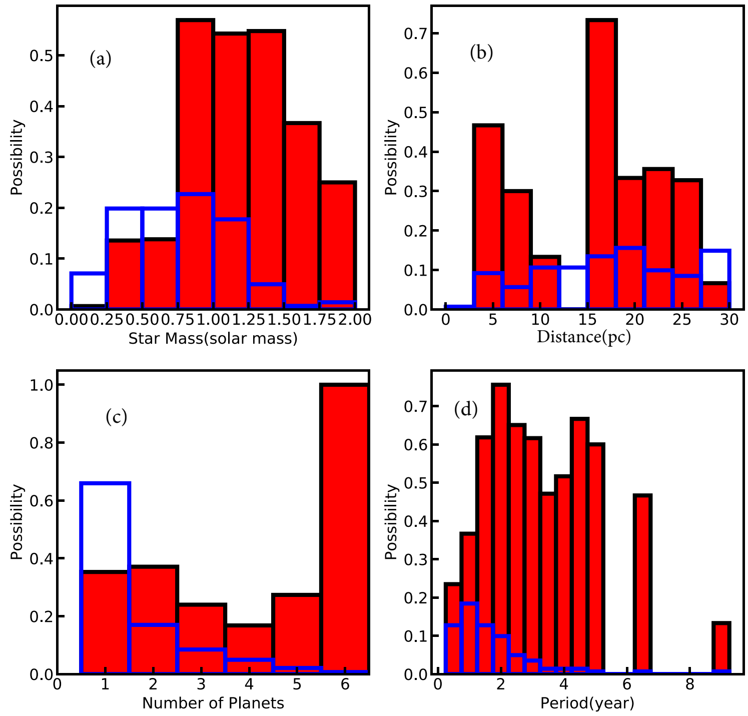

Fig. 5 The *red bars* are the statistics of probability $P_{\rm HP4}$ for all the selected 140 systems, correlated to (a) the stellar mass, (b) the distance, (c) the number of known planets and (d) the period of the planets in HZ. The *blue lines* represent the fraction of planets systems in our sample.

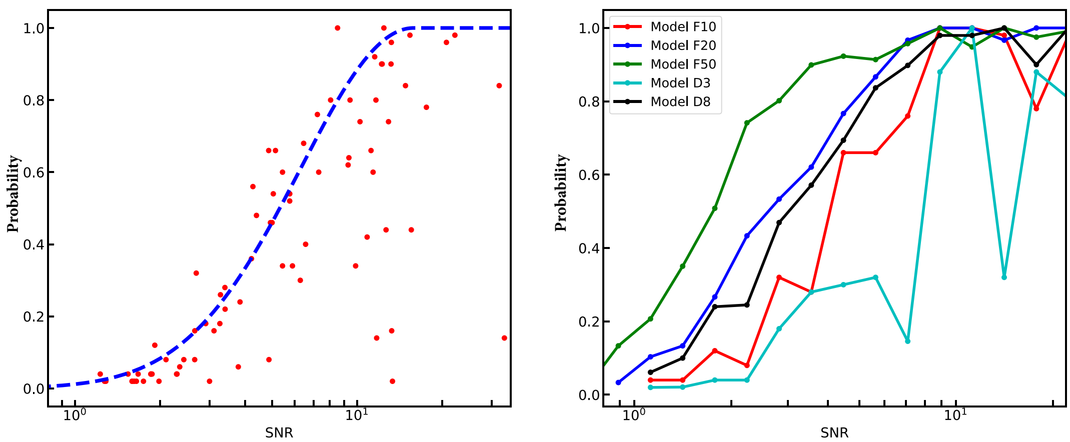

Fig. 6 In the left panel, the *red dots* are the simulation results in Mode F10 or D5, while the *blue line* is potted via theoretical equation (8) in paper I. The detection probabilities in five observation modes adopted in this paper are plotted in the right panel.

region of $2 \leq F \leq 25$ and $1 \leq D \leq 16$, the difference is less than 20%. Combining with the expressions of $P_{\rm SNR}$ and $P_{\rm S}$ in Yu et al. (2019), we can use the empirical Equation to estimate the detection probability $P_{\rm HP4}$ in Equation 10 for a certain planet systems, i.e.,

$$\begin{aligned} P_{\rm HP4} =& P_{\rm SNR} P_{\rm S} (0.040F - 0.021) \\ & \times (0.058D^2 + 0.340D - 0.216)\,. \end{aligned} \tag{16}$$

We note that if only one habitable planet is present in the system, $P_{\rm S}$ equals 1. According to Equation (15), a value of larger than one is allowed for P_3, thus $P_{\rm HP4}$ is also possible to be larger than 1. We adopt a maximum value of 1 for $P_{\rm HP4}$, which is very rare in our simulations.

3.3 Applications in Known Planetary Systems

We investigate three typical planetary systems, namely M star systems with only one planet detected in HZ like PC; systems like HD 189733 with one hot Jupiter; and systems similar to HD 102365, with one warm Neptune. We will demonstrate how to estimate the requirements of

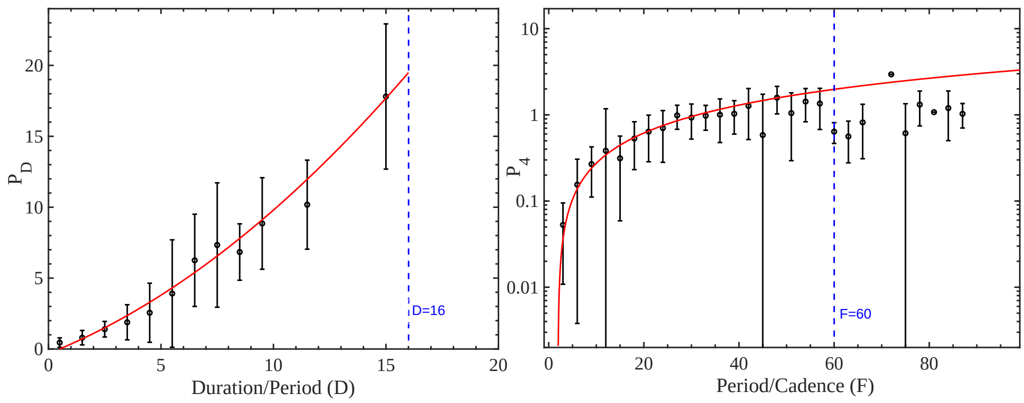

Fig. 7 The left panel: *black circles* show the averaged P_3 around different $D = \mathrm{Duration/Period}$, a quadratic function can fit the data well as the *red line*. The right panel: *black circles* show the averaged P_4 around different $F = \mathrm{Period/Cadence}$, a linear fit is good enough for $F < 60$.

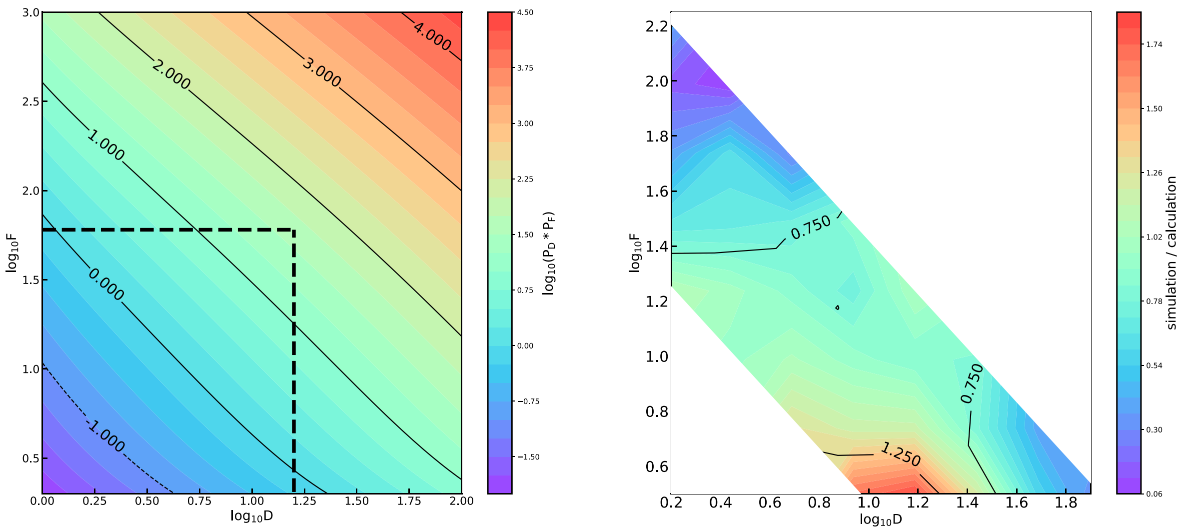

Fig. 8 The left panel is the detection probability as a function of D and F, according to the expression of the last two terms in Eq. (15). The *black dashed line* is the region of $1 \leq D \leq 16$ and $2 \leq F \leq 60$. The color represents the value of the detection probability. The right panel is the fitting error between the calculated value and the value form the simulation results. The color represents the simulation results divided by the calculated results. The contour lines is the 0.75 and 1.25 means the fitting error is <25%.

observations for these three types of systems, based on Equation (15).

For the PC system, the known planet in HZ has a very short period of ∼11.18 day, which is too short for Mode f50 to determine the period correctly because the F value is smaller than 2, as seen in Table 1, where P_{HP} is 0. If the frequency is increased to, for example, 100 measurements per year, however, the period of the planet can be well retrieved. The SNR of PC b is about 2, based on Equation (2), and $P_{\mathrm{S}} = 1$ because it is a single planet system. Assuming F is 3, to achieve a detection probability of 90%, $D \geq 40$ is required, according to Equation (15). We note that Equation (15) can only be applied when $1 \leq D \leq 16$, and in the region of $D \geq 40$ with $F = 3$, the calculated probability should be larger than the real value, as shown in Figure 8. Therefore, even for $D = 40$, the detection probability is still less than 90%, meaning the observation should last longer than 40 periods (about 1.2 year). If PC is only observed for half a year, in which case D equals to 16, F should then be larger than 9.6 to guarantee $P_{\mathrm{HP4}} = 90\%$.

HD 189733 has a hot-Jupiter with a period of 2.22 day. According to the definition of SNR and P_{S}, the former one is estimated to be 2.9, and the latter one 0.689 for an injected planet in HZ with a period of 0.91 year. In Mode f10 or f5, P_{HP4} is only 18%, if a much higher detection probability such as 90% is required, F needs to be larger than 43 during a 5-year mission, according to Equation (15). If the data cadence is fixed at 0.1 years, the value for D should be 14.6, indicating the mission time should be longer than 13.25 years, which is very challenging for HEPS.

HD 102365 is a system with a warm Neptune with a period of ∼122 day. The SNR is 16.8, and $P_{\rm S}$ equals to 0.748 for an added planet in HZ with a period of 1.02 year. In Mode f10 or D5, the detecting probability is about 78%. If a detection probability of larger than 90% is expected, F needs to be larger than12 during a 5-year mission. Fixing the data cadence at 0.1 years, D needs to be at least 6 to achieve a probability of 90%, which means the lifetime of HEPS should be longer than 5.7 years.

4 CONCLUSIONS AND DISCUSSIONS

In this work, we focus on the sub-μas astrometry precision of next generation space telescope (i.e., HEPS) to test its ability to detect Earth-like planets in HZs around nearby planet hosts. In Section 2, we selected a sample of 140 planet hosts within 30 pc as the potential targets for HEPS. We estimated the HZs according to the updated parameters of the host stars, injected a 10 earth-mass planet in the HZs around some of the host stars, and checked the stability of the systems. Then, we simulated the astrometric signals including a random white noise based on the brightness of the host stars.

In Section 3, we adopted five different modes with different observation durations and cadences in our simulations; that is, 10, 20 and 50 measurements per year for 5 years, and 10 measurements per year for 3 and 8 years. Using the fitting procedures introduced in Section 2, we calculated the detection probabilities of the planets in HZ of each system, based on the precision of planet mass, period, eccentricity, and inclination. Combining with the stability of the system, we estimated the total detecting probability of planet in HZ-P_t.

In Section 3.1, all of the systems in our sample are listed in Table 1 and are ranked by descending detection probability- $P_{\rm HP4}$ of Mode f10/d5. According to Table 1, we are able to choose target stars for HEPS, which probably own detectable planets in HZ. 16 systems with high detecting probabilities of planet in HZ are listed in Table 3 for different observational modes. We demonstrate that planets in HZ around solar-like stars with $0.75-1.5$ solar mass are preferred to be detected. Injected planets with periods of $1-5$ years, or in systems with fewer detected planets are also preferred to be detected, as shown in Figure 5.

In Section 3.2, we choose parameters F and D in Equation (11) to investigate the influence on the detecting probability- $P_{\rm HP4}$ due to data cadence and observational duration, respectively. According to our simulations, we fit the enhanced factor $f(D,F)$ (i.e.) $P(3)$, to model the influence on $P_{\rm HP4}$, as shown in Equation (15). The fitting results are available for systems with $2 \leq F \leq 25$ and $1 \leq D \leq 16$, where the differences between the empirical and simulated results are relatively small. Combining with the correlation between $P_{\rm HP4}$ and SNR and the orbital architecture of multi-planet systems in Yu et al. (2019), we can estimate $P_{\rm HP4}$ for a certain system using Equation (16) in different observational modes.

In Section 3.3 we took PC, HD 189733, and HD 102365 for instance, to show how to use Equation (16) to optimize the observational modes. If we wish to detect PC b, with a data cadence of 3.76 day (i.e., $F=3$), at least an observation time of 1.2 years is required to achieve a detecting probability larger than 90%. Instead of the typical observational Mode f10 or D5 of HEPS, smaller data cadence are beneficial to enhance the probability of systems with hot Jupiter or warm Jupiter, such as systems similar to HD 189733 and HD 102365.

However, some assumptions need further studies. Firstly, we assume an injected planet in HZ of each planet host. However, the occurrence rate of planet in HZ is still unknown. Dressing & Charbonneau (2015) estimates the occurrence rate of habitable planets around M stars based on Kepler data, and concludes that about 16% M dwarfs contain Earth-size planets in their HZs, and 12% M dwarfs contain super-Earths in their HZs. For GK dwarf stars, (Burke et al. 2015) shows 0.1 terrestrial planets per Kepler GK dwarf star on average, with periods from 0.8 to 1.2 years. However, the uncertainty of the average planet number in HZ is extremely large (i.e., from 0.01 to 2). More observations from TESS might reveal the occurrence rate of planet around nearby stars. Secondly, in our simulations, we adopt even cadences in different modes to generate astrometric signals. However, uneven cadence would enhance the coverage of the orbital phase, which benefits the retrieval of the planet parameters. Additionally, the simulated signals only include a white noise model based on the brightness of the star. Realistically, red noise is common and crucial to the detection of planets in HZ, which needs to be modeled during the instrument test.

In this work, we ignore the influence of the binaries. Binaries would cause more complex motion of the host stars. In our results, we have not individually studied of the detection probability of planets with periods of one year. Consequently, we aim to make a more detailed research on the influence of binary and the period of planet in future work.

The final data release of Gaia may reveal some gas giants around nearby stars, which will increase the number of stars in the sample of planet hosts, and the method in this work can then be extended to estimate the probability of detecting planets in HZ of these systems. Additionally, there are RV measurements for nearby bright stars. Combining RV data and transit data, the more complete set of parameters of known planets could be calculated more precisely, which would benefit the detection of planets in HZs.

Acknowledgements This work is supported by the National Natural Science Foundation of China (Grant Nos. 11503009, 11973028, 11933001, 11673011 and 11803012). We also thank the Qian Xuesen Laboratory initiative research program and the Technology of Space Telescope Detecting Exoplanet and Life supported by the National Defense Science and Engineering Bureau civil spaceflight advanced research project D030201. Ensi Liang is grateful to the support of Program A for Outstanding PhD candidates of Nanjing University.

References

Anglada-Escudé, G., Amado, P. J., Barnes, J., et al. 2016, Nature, 536, 437
Burke, C. J., Christiansen, J. L., Mullally, F., et al. 2015, ApJ, 809, 8
Chambers, J. E., Wetherill, G. W., & Boss, A. P. 1996, Icarus, 119, 261
Chen, D., Wu, J., & Li, B. 2013, European Planetary Science Congress, EPSC2013-1102
Dressing, C. D., & Charbonneau, D. 2015, ApJ, 807, 45
Eggl, S., Pilat-Lohinger, E., Georgakarakos, N., Gyergyovits, M., & Funk, B. 2012, ApJ, 752, 74
Fehlberg E. 1968, NASA Tech Rep R-287, `https://ntrs.nasa.gov/archive/nasa/casi.ntrs.nasa.gov/19680027281.pdf`
Gaia Collaboration, Prusti, T., de Bruijne, J. H. J., et al. 2016, A&A, 595, A1
Gaia Collaboration, Brown, A. G. A., Vallenari, A., et al. 2018, A&A, 616, A1
Gillon, M., Jehin, E., Lederer, S. M., et al. 2016, Nature, 533, 221
Haghighipour, N., & Kaltenegger, L. 2013, ApJ, 777, 166
Konopacky, Q. M., Rameau, J., Duchêne, G., et al. 2016, ApJ, 829, L4
Kopparapu, R. K., Ramirez, R., Kasting, J. F., et al. 2013, ApJ, 765, 131
Malbet, F., Léger, A., Shao, M., et al. 2012, Experimental Astronomy, 34, 385
Marquardt, Donald W. 1963, Journal of the Society for Industrial and Applied Mathematics, 11, 431, `https://doi.org/10.1137/0111030`
Perryman, M., Hartman, J., Bakos, G. Á., & Lindegren, L. 2014, ApJ, 797, 14
Ribas, I., Tuomi, M., Reiners, A., et al. 2018, Nature, 563, 365
Shao, M. 2019, American Astronomical Society Meeting, 51, 212.04
The Theia Collaboration, Boehm, C., Krone-Martins, A., et al. 2017, arXiv e-prints (arXiv:1707.01348)
Tuthill, P., Bendek, E., Guyon, O., et al. 2018, Proc. SPIE, 107011J
Unwin, S. C., Shao, M., Tanner, A. M., et al. 2008, PASP, 120, 38
Wright, J. T., & Howard, A. W. 2009, ApJS, 182, 205
Yu, Z.-Y., Liu, H.-G., Zhou, J.-L., et al. 2019, RAA (Research in Astronomy and Astrophysics), 19, 004